150-kW Three-Port Custom-Core Transformer Design Methodology

Shamar Christian*, Roberto Armin Fantino*, Roderick Amir Gomez*, Juan Carlos Balda*, Yue Zhao*, Guangqi Zhu†
*Department of Electrical Engineering, University of Arkansas, Fayetteville Arkansas, USA
†Eaton Research Labs, Menomonee Falls, Wisconsin, USA
sc114@uark.edu, rafantin@uark.edu, ragomezj@uark.edu, jbalda@uark.edu, yuezhao@uark.edu

***Abstract*— The design of a 150-kW high-frequency three-port transformer (TPT) for a triple active bridge (TAB) converter application is the focus of this paper. A non-tradeoff inclusive design methodology for custom-core transformers is proposed. Classic transformer design methodologies based on complex trade-offs mechanisms require significant effort to adjust the design for commercially available pre-sized cores. The proposed design is based on the development of a set of design equations that allows to select the core dimensions and the turns numbers for the windings that best accomplish the transformer specifications. Experimental evidence verifying the proposed theoretical design methodology is presented in this work.**

Keywords*— *Transformer, windings, high frequency, optimum design, nanocrystalline, high efficiency

I. Introduction

Renewable energy distribution is greatly depends upon the development and reliability of power electronic high-power conversion systems [1], [2]. In general, these systems require the use of transformers to meet galvanic isolation requirements. Development of high-efficiency high-frequency transformers is a growing trend to pursue size reductions and increasing power densities [3], [4]. Typical transformer design methodologies involve the implementation of cumbersome trade-off design algorithms that should be adjusted to commercially available pre-sized cores [3]–[7]. Recent developments in manufacturing capabilities of core materials allow for producing geometrically customized cores. This work assesses the design of a 150-kW TPT for a TAB converter [8]–[10]. A design methodology that allows an optimized selection of a customized core avoiding undesirable trade-offs when using commercial cores is proposed. By developing a set of equations depending only on one core dimension and the number of turns of one winding, the best solution for these two parameters will define all the remaining transformer characteristics. The proposed method is verified by building and testing the designed transformer.

II. Operating Conditions of TPT in TAB

A. Operating conditions of TPT in the TAB

Figure 1(a) shows the circuit of a TAB [8]–[11]. The input stage DC voltages V_{in1} and V_{in2} feed two full-bridge (FB) converters whose AC output voltages v_{p1} and v_{p2} inject the currents i_{p1} and i_{p2} to the TPT primaries through the external

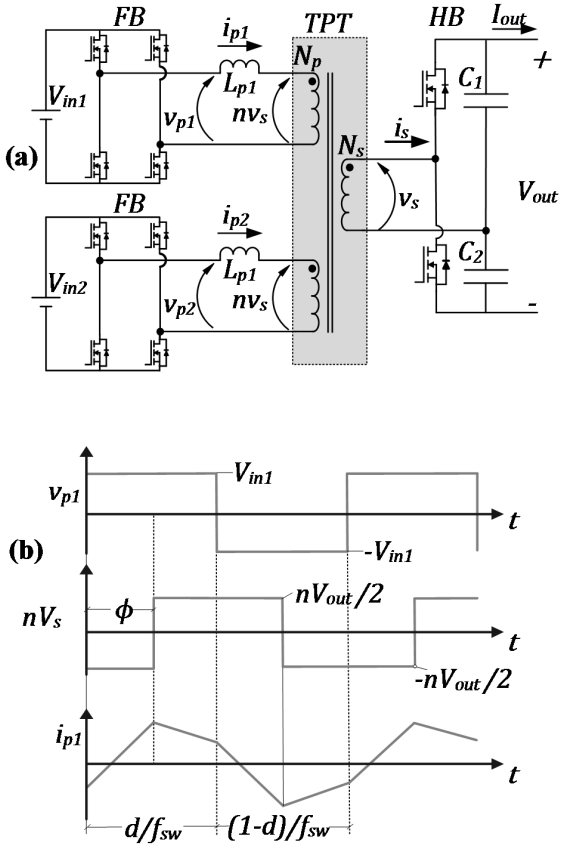

Fig. 1: (a) TAB topology. (b) Main theoretical TPT waveforms at rated power.

inductors L_{p1} and L_{p2} (whose design is outside the scope of this work). The TPT turns ratio is $n = N_p/N_s$, where N_p and N_s are the numbers of turns of the two primaries and the secondary, respectively. The TPT AC output voltage v_s, feeds the current i_s to the half-bridge (HB) converter stage with a fixed controlled DC output voltage V_{out}. The three converters operate at a switching frequency f_{sw} and a fixed duty cycle $d = 0.5$.

III. TPT Design Methodology

A. Selection of Magnetic Core material and Wire

The TPT design begins with the magnetic core material and winding wire selection. Fig. 2 shows the considered E type core transformer structure with core geometric

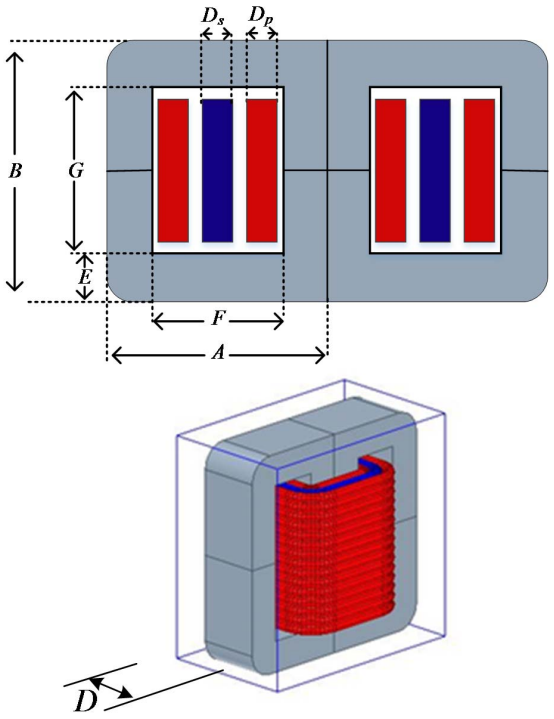

Fig. 2 Transformer structure and dimensions

dimensions (A, B, F, G, D, E). It is selected $E = D/2$ to have a square shape central leg. Each winding is built in a single layer to reduce losses and leakage inductance, with the secondary winding placed between the two primaries (concentrically wound) [12]. To reduce high-frequency skin effect losses, S_p and S_s strands of Litz wire with cross section area A_{litz} [13], are used for the primaries and secondary, respectively. Let $A_p = \delta A_{litz} S_p$ and $A_s = \delta A_{litz} S_s$ be the total areas of the two primaries and secondary windings, respectively, where δ is the wire fill factor (including insulation). The total diameter of the wires can be expressed as $D_p = 2\sqrt{A_p/\pi}$ and $D_s = D_p\sqrt{S_s/S_p}$. The mean lengths per turn of the primaries and the secondary can be estimated as $l_{p1} = 4(D + D_p)$, $l_{p2} = 4\left[D + \left(3 + 2\sqrt{S_s/S_p}\right)D_p\right]$, $l_s = 4\left[D + \left(2 + \sqrt{S_s/S_p}\right)D_p\right]$. Remaining dimensions are $F = D_p\left(2 + \sqrt{S_s/S_p} + K_{ext}\right)$, $A = (F + D)$, $G = D_p(N_p + K_{ext})$ and $B = (G + D)$, where $K_{ext} = 1$ is a coefficient used to leave extra space $D_{ext} = K_{ext} D_p$ for the wire insulation and bobbin.

B. Copper Losses, Core Losses and Temperature Rise

Design equations depending only on N_p and D are developed. Due to Litz wire utilization, the AC resistance of the windings can be considered approximately equal to its DC resistance [14]. Hence, an estimation of the copper losses in the windings are made as follows:

$$P_{cu} = \frac{\rho_{cu} N_p}{A_{litz}}\left[\frac{(l_{p1}+l_{p2})}{S_p} I_p^2 + \frac{l_s}{nS_s} I_s^2\right] = k_{cu}\left[D + D_p\left(2 + \sqrt{S_s/Sp}\right)\right], \quad (1)$$

where I_p and I_s are the rms values of i_p and i_s respectively, $\rho_{cu} = 1.68 \times 10^{-8}\Omega/m$ and $k_{cu} = (4\rho_{cu} N_p/A_{litz})\left[2I_p^2/S_p + I_s^2/(nS_s)\right]$. A square-wave voltage magnetizing the TPT (see nv_s in Fig.1) will produce a triangular flux density waveform with peak value $B_{max} = V_{max}/(4 f_{sw} N_p A_c)$ [15], [16]. Core losses are estimated by using the Improved Generalized Steinmetz Equation [4], [15], [16]:

$$P_{fe} = V_{fe} k_i f_{sw}^{\alpha} B_{max}^{\beta}$$

with

$$k_i = \frac{2^{(\alpha+1)} K_c}{\pi^{(\alpha-1)}\left(1.1044 + \frac{6.8244}{\alpha + 1.354}\right)} \quad (2)$$

where α, β and K_c are the core Steinmetz coefficients. In (2), the core volume can be expressed as $V_{fe} = 2D^2\left[D + D_p(5 + N_p)\right]$, with $A_c = D^2 K_{eff}$ being the core effective cross-sectional area, and K_{eff} the core stacking factor. By combining (1) and (2), the total TPT losses are given by:

$$P_T = k_{fe} D^{2(1-\beta)} N_p^{-\beta}\left[D + D_p(5 + N_p)\right] + \cdots \ldots k_{cu}\left[D + D_p\left(2 + \sqrt{\frac{S_s}{S_p}}\right)\right], \quad (3)$$

where $k_{fe} = \left[2^{(1-2\beta)} f_{sw}^{(\alpha-\beta)} V_{max}^{\beta} K_{eff}^{-\beta} k_i\right]$. Note that in (3), N_p and D are the only two parameters needed to be selected, while the remainder are system parameters or previously determined core material and wire parameters. To obtain an estimate of the transformer rise in temperature, the basic relationship for heat transfer by convection $P_T = hA_{surf}\Delta T$ is used [17], where ΔT is the rise in temperature of the TPT surface (of area A_{surf}) with respect to the ambient, and h is an empirical heat transfer coefficient ($h = 22\ W/m^2$ is used in this work). By using the sum of the core and winding volumes $V_{fecu} = V_{fe} + V_{cu}$, with $V_{cu} = \pi D_p^2 N_p\left[2 + S_s/(nS_p)\right]\left[D + \left(2 + \sqrt{S_s/S_p}\right)D_p\right]$, the simplified expression $A_{surf} \approx \sqrt[3]{36\pi V_{fecu}^2}$ that corresponds to the surface area of a sphere with a volume V_{fecu} is generated. By inserting the losses from (3), the transformer surface rise in temperature can be estimated by:

$$\Delta T \approx \frac{k_{fe} D^{2(1-\beta)} N_p^{-\beta}\left[D + D_p(5 + N_p)\right] + k_{cu}\left[D + D_p\left(2 + \sqrt{\frac{S_s}{S_p}}\right)\right]}{h_c \sqrt[3]{36\pi}\left\{2D^2\left[D + D_p(5 + N_p)\right] + \pi D_p^2 N_p\left[2 + \frac{S_s}{nS_p}\right]\left[D + \left(2 + \sqrt{\frac{S_s}{S_p}}\right)D_p\right]\right\}^{2/3}} \quad (4)$$

Furthermore, it is desirable to limit the total transformer volume V_T that it will occupy in a cabinet:

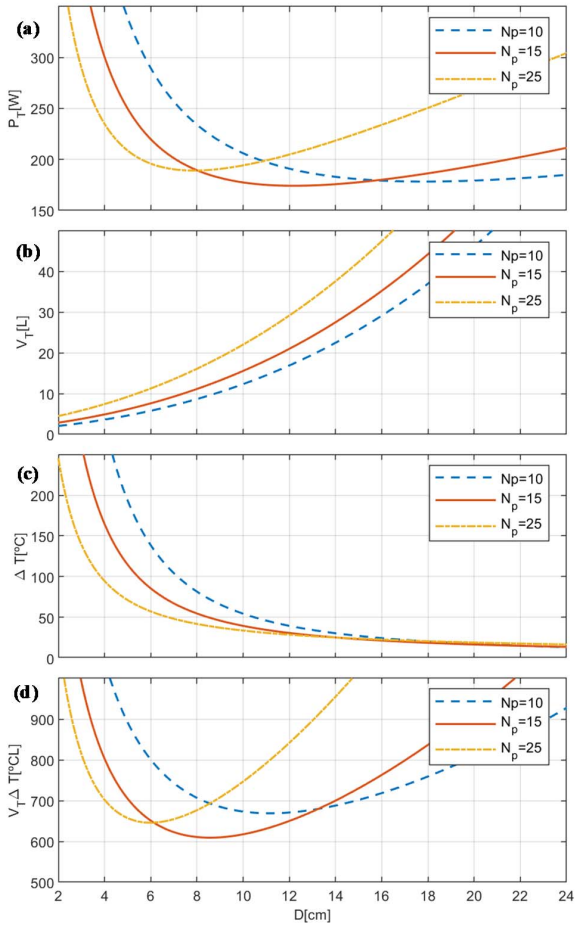

Fig. 3(a) P_T[W]. (b) V_T[L]. (c) ΔT[ºC]. (d) $V_T \Delta T$

$$V_T = D^2\left[2D + D_p\left(N_p + 2\sqrt{S_s/S_p} + 7\right)\right] + \ldots$$
$$\ldots\ D_p\left(N_p + 1\right)\left[D + 2D_p\left(3 + \sqrt{\frac{S_s}{S_p}}\right)\right]\left[D + 2D_p\left(2 + \sqrt{\frac{S_s}{S_p}}\right)\right] \quad (5)$$

Unlike V_{fecu}, V_T additionally considers the extra space volume for bobbin and insulation.

TABLE I. SYSTEM SPECIFICATIONS

Symbol	Value
n	1
f_{sw}	20 kHz
η	> 99.6 %
J_{max}	3A/mm^2
V_{in} ; V_{out}	1.3 kV ; 2.6 kV
I_{smax}; I_{pmax}	135Arms; 67.5Arms
V_T	< 20 L
ΔT	<100 °C

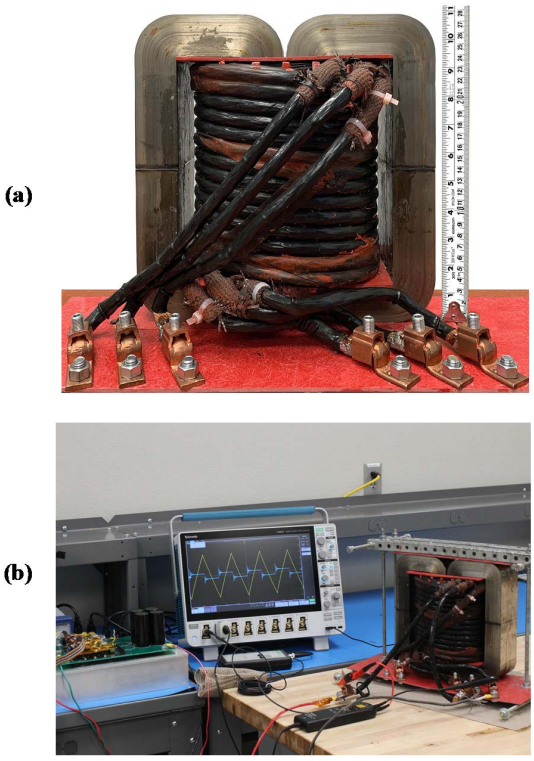

Fig. 4(a) Designed *TPT*. (b) Experimental setup.

IV. TRANSFORMER PROTOTYPE DESIGN

In this section, a TPT for a TAB with the specifications listed in Table I is designed. Because of its advantages considering design requirements [5], [18], [19], nanocrystalline core material with the parameters listed in Table II is selected. To satisfy J_{max}, commercially-available Litz wire with 4000 strands of $A_{litz} = 0.0131mm^2$ (adequate for $f_{sw} = 20kHz$) is selected. With the aim of keeping copper losses and low building complexity low, this wire is selected for all windings, resulting $S_s/S_p = 1$ and $D_p = 12.39$mm. Having selected the core material and the wire, the equations presented in Section III can be analyzed in order to select the parameters N_p and D that best satisfy the TPT design requirements. For the converter operating at nominal conditions and maximum power transferred $P_o = 150$kW, Fig. 3 (a) illustrates P_T (3), evaluated for three values of N_p (10, 15 and 25), and for $2cm < D < 24cm$. Similarly, Fig. 3 (b) displays the total volume V_T (5), and Fig. 3 (c) shows the temperature rise ΔT (4). Minimum P_T is the target usually considered in transformer design [15], however this does not occur at optimum values of V_T.

TABLE II. CORE CHARACTERISTICS

Symbol	Value
α	1.2077
β	1.6456
K_c	2.2991 W/m^3
K_{eff}	0.78

The goals in this work are to minimize ΔT to avoid introducing system losses requiring complex cooling methods [3], and to minimize V_T for cost and size reductions. To consider these goals (oppositely related through D), the cost function ΔTV_T plotted in Fig. 3 (d) is analytically obtained by evaluated by multiplying equation (4) and (5). For each N_p, there is a value of D for which ΔTV_T has a minimum, and there is a global minimum for a particular N_p.The set of N_p and D that minimizes ΔTV_T can be. For the current design, the minimum occurs for $N_P = 15$ and $D \approx 8$ cm. By selecting these values, the remaining core parameters are determined following the procedure presented in section III. The resultant designed TPT, with a theoretical efficiency of η_{th} =99.875%, has been constructed and it is shown in Fig. 4(a).

The TPT design methodology can be summarized as follows:

- Select core material and geometry.
- Select winding wires based on operating frequency and J_{max} requirement.
- Express core and winding dimensions based on N_p and D.
- Compute (3), (4) and (5) through iterations of N_p and D.
- Select the values of N_p and D that best accomplish design targets. In the presented design, the solution minimizing the cost function ΔTV_T has been selected.

V. Experimental Results

In order to calculate the losses produced in the constructed TPT, open-circuit (OC) at nominal voltage operation and short-circuit (SC) at nominal current operation were performed by using an available 2000V – 100A FB converter. The picture in Fig.4(b) displays part of the experimental setup used to implement the tests. Supporting waveforms of current and voltage for the OC and SC tests are shown in Fig. 5(a) and Fig. 5(b) respectively. For an applied nominal 1300V square wave, core losses equal to $P_{oc} = 129$ W were measured in the OC test, corresponding to a $R_m = (1300V)^2/129W \approx 13$ kΩ magnetizing resistance. By using the slope of the OC current shown in Fig. 5(a), a $L_m \approx 12.5$ mH magnetizing inductance can be calculated. For the same conditions, the theoretical losses obtained by using (2) results in $P_{fe} = 118$ W, the difference could be attributed to a slight error in the used core Steinmetz coefficients or staking factor. By using the measured OC losses in (4), $\Delta T \approx 31°C$ is expected in the OC test, close to the rise in temperature $\Delta T \approx 27°C$ that can be seen in the thermal image given in Fig. 4(c). The SC test was implemented for a $I_{sc} \approx 67.5A_{rms}$ current applied to one of the primaries with the secondary short-circuited. For this test, the measured losses were $P_{sc} \approx 100$ W, so the resistance of the two windings in series can be calculated as $R_{sc}=P_{sc}/I_{sc}^2 \approx 20$mΩ . By assuming that the two windings have the same impedance, the per winding series resistance can be approximated as $R_s \approx 10$ mΩ. The slope of the SC current shown in Fig. 5(b), corresponds to a per winding leakage inductance of $L_{lk} \approx 3.5\ \mu H$. By using the estimated per winding resistance, the copper losses in the three winding for the TPT operating

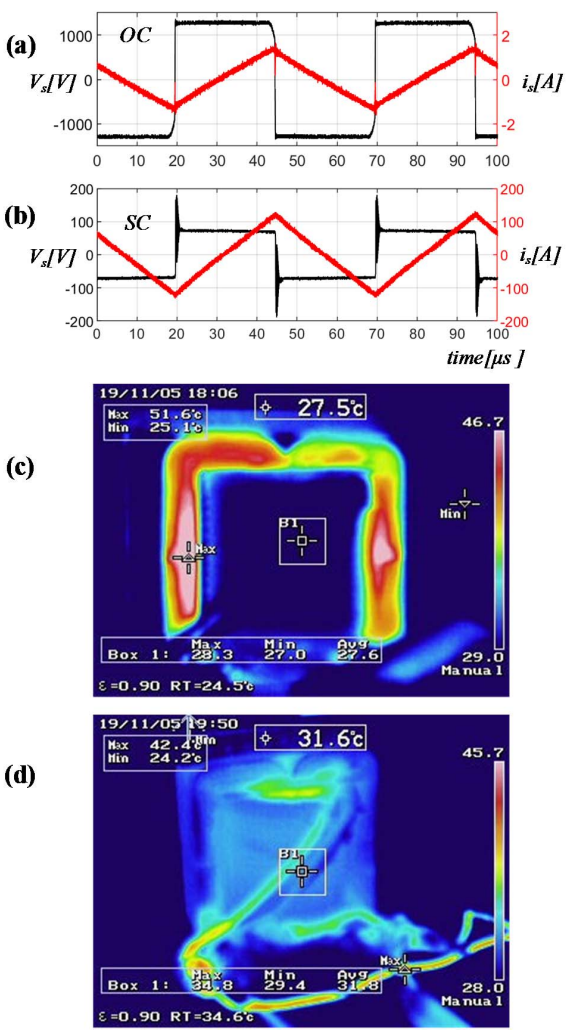

Fig. 5: (a) OC Test Waveform. (b) SC Test Waveform. (c) Thermal image for OC. (c) Thermal image for SC.

under nominal conditions can be estimated as $P_{cu} \approx (2I_{pmax}^2 + I_{smax}^2)R_s \approx 273$W , then expected total losses at rated power are $P_T = P_{oc} + P_{cu} \approx 402$W , yielding an efficiency of $\eta = 99.73\%$, satisfying the design specifications given in Table I.

VI. Conclusions

A design methodology for a custom-core transformer design was proposed and experimentally verified for the design of a 150-kW 20-kHz three-port transformer for a triple active bridge converter application. The open-circuit and short-circuit tests were implemented on the constructed transformer at nominal voltage and current ratings, producing results very close to the theoretically calculated values. In accordance with the obtained results, a high efficiency of 99.73% is expected for the transformer operating at nominal conditions. Future work involves extending comprehensive experimental

testing of the transformer working within the TAB converter system to further validate the proposed ideas.

ACKNOWLEDGMENT

This material is based upon work by the U.S Department of Energy´s Office of Energy Efficiency and Renewable Energy (EERE) under Solar Technologies Office (SETO) Agreement Number EE0008349.

REFERENCES

[1] V. Yaramasu, B. Wu, P. C. Sen, S. Kouro, and M. Narimani, "High-power wind energy conversion systems: State-of-the-art and emerging technologies," *Proc. IEEE*, vol. 103, no. 5, pp. 740–788, May 2015.

[2] G. Spagnuolo *et al.*, "Renewable Energy Operation and Conversion Schemes: A Summary of Discussions During the Seminar on Renewable Energy Systems," *IEEE Ind. Electron. Mag.*, vol. 4, no. 1, pp. 38–51, 2010.

[3] M. Leibl, G. Ortiz, and J. W. Kolar, "Design and Experimental Analysis of a Medium-Frequency Transformer for Solid-State Transformer Applications," *IEEE J. Emerg. Sel. Top. Power Electron.*, vol. 5, no. 1, pp. 110–123, Mar. 2017.

[4] M. Mogorovic and D. Dujic, "100 kW, 10 kHz Medium-Frequency Transformer Design Optimization and Experimental Verification," *IEEE Trans. Power Electron.*, vol. 34, no. 2, pp. 1696–1708, Feb. 2019.

[5] O. Aldosari, L. A. Garcia Rodriguez, J. C. Balda, and S. K. Mazumder, "Design Trade-Offs for Medium- and High-Frequency Transformers for Isolated Power Converters in Distribution System Applications," in *2018 9th IEEE International Symposium on Power Electronics for Distributed Generation Systems (PEDG)*, 2018, pp. 1–7.

[6] Juanjuan Zhang, Yumei Du, Zixin Li, and Ping Wang, "Design of a medium frequency, high voltage transformer for power electronic transformer," in *2014 IEEE Conference and Expo Transportation Electrification Asia-Pacific (ITEC Asia-Pacific)*, 2014, pp. 1–5.

[7] G. Ortiz, M. Leibl, J. W. Kolar, and O. Apeldoorn, "Medium frequency transformers for solid-state-transformer applications — Design and experimental verification," in *2013 IEEE 10th International Conference on Power Electronics and Drive Systems (PEDS)*, 2013, pp. 1285–1290.

[8] L. Jiang and D. Costinett, "A triple active bridge DC-DC converter capable of achieving full-range ZVS," in *2016 IEEE Applied Power Electronics Conference and Exposition (APEC)*, 2016, pp. 872–879.

[9] R. Liu, L. Xu, Y. Kang, Y. Hui, and Y. Li, "Decoupled TAB converter with energy storage system for HVDC power system of more electric aircraft," *J. Eng.*, vol. 2018, no. 13, pp. 593–602, 2018.

[10] V. N. S. R. Jakka, A. Shukla, and S. V Kulkarni, "Flexible Power Electronic Converters for Producing AC Superimposed DC (ACsDC) Voltages," *IEEE Trans. Ind. Electron.*, vol. 65, no. 4, pp. 3145–3156, Apr. 2018.

[11] L. Piris-Botalla, G. G. Oggier, A. M. Airabella and G. O. García, "Extending the operating limits of a bidirectional three-port DC-DC converter," *2015 XVI Workshop on Information Processing and Control (RPIC)*, Cordoba, 2015, pp. 1-6.

[12] M. Michon, J. L. Duarte, M. Hendrix, and M. G. Simoes, "A three-port bi-directional converter for hybrid fuel cell systems," in *2004 IEEE 35th Annual Power Electronics Specialists Conference (IEEE Cat. No.04CH37551)*, 2004, vol. 6, pp. 4736-4742 Vol.6.

[13] L. Dixon, "Eddy Current Losses in Transformer Windings and Circuit Wiring," *Unitrode Semin. Man. SEM600*, 1988.

[14] C. William and T. McLyman, *Transformer and Inductor Design Handbook*. Taylor & Francis Group, 2011.

[15] V. Väisänen, J. Hiltunen, J. Nerg, and P. Silventoinen, "AC resistance calculation methods and practical design considerations when using litz wire," in *IECON 2013 - 39th Annual Conference of the IEEE Industrial Electronics Society*, 2013, pp. 368–375.

[16] W. G. Hurley and W. W. H., *Transformers and Inductors for Power Electronics: Theory, Design and Applications*. John Wiley & Sons, 2013.

[17] J. Muhlethaler, J. Biela, J. W. Kolar, and A. Ecklebe, "Improved Core-Loss Calculation for Magnetic Components Employed in Power Electronic Systems," *IEEE Trans. Power Electron.*, vol. 27, no. 2, pp. 964–973, Feb. 2012.

[18] J. H. Lienhard, *A Heat Transfer Textbook*. Dover Publications, 2011.

[19] R. Burdt *et al.*, "Evaluation of Nanocrystalline Materials, Amorphous Alloys and Ferrites for Repetitive-Magnetic Pulse Compression Applications," in *2005 IEEE Pulsed Power Conference*, 2005, pp. 843–847.

[20] T. Kauder and K. Hameyer, "Performance Factor Comparison of Nanocrystalline, Amorphous, and Crystalline Soft Magnetic Materials for Medium-Frequency Applications," *IEEE Trans. Magn.*, vol. 53, no. 11, pp. 1–4, Nov. 2017.